Laser and Particle Beams (2017), *35*, 145–153.

doi:10.1017/S0263034616000896

Absolute equation of state measurement of aluminum using laser quasi-isentropic-driven flyer plate

H. SHU, X. HUANG, J. YE, G. JIA, J. WU, AND S. FU
Shanghai Institute of Laser Plasma, Shanghai 201800, China
(RECEIVED 12 August 2016; ACCEPTED 15 December 2016)

Abstract

In this paper, we perform an absolute equation of state (EOS) measurement on the principal Hugoniot of aluminum using a near-symmetric impact method. The flyer plates are accelerated to high velocities using the laser-ramp-driven method. An aluminum flyer plate of ~25 μm is accelerated to the velocity range from 4 to 12 km/s. Then the aluminum flyer plate propagates across a vacuum gap and impacts with an aluminum step target. A line-imaging optical recording velocity interferometer for any reflector (ORVIS) is used to measure the aluminum flyer plate and the shock velocity simultaneously. Aluminum EOS data were measured with pressures range from 50 to 200 GPa. This absolute EOS measurement method may be used for studying a variety of materials.

Keywords: equation of state; Hugoniot; laser

1. INTRODUCTION

Equation of state (EOS) data of matter in high-pressure regime is a subject of interest for many fields of modern physics (Benuzzi *et al.*, 1996; Gu *et al.*, 1996; Celliers *et al.*, 1998; GODWAL *et al.*, 2003; Batani *et al.*, 2004; Batani, 2016), including astrophysics and geophysics. In particular, in the ICF (inertial confinement fusion) (Hann *et al.*, 1995; Lindl, 1995; Koenig *et al.*, 1998) researches, compression efficiency, and shock structure in fusion capsules critically depend on the EOS. In the past, TPa pressures can be achieved by strong shock waves driven with high-energy pulse powers such as nuclear explosions (Ragan, 1982; Vladimirov, 1984; Mithcell *et al.*, 1991). Recently, laser-driven shock waves provided EOS data for a variety of materials used in high-energy-density physics experiments at pressures above 1 Mbar. Most of the EOS studies using laser drive shocks rely on impedance matching to determine the behavior of a sample by comparing it to a known standard. At very high pressures (>5 Mbar), uncertainties in the EOS of that standard material ultimately limit the accuracy of this technique. So far, very few absolute EOS (Silva *et al.*, 1997; Cauble *et al.*, 1998; Benuzzi-Mounaix *et al.*, 2002) experiments were reported using the laser-driven shock wave method. In these experiments, two shock physical quantities of the shocked matter are determined simultaneously (the shock speed and the particle speed). For the low *Z* materials, the particle velocity can be measured using time-resolved X-ray radiography (Silva *et al.*, 1997; Cauble *et al.*, 1998). For the high *Z* materials, the particle velocity can be inferred from the rear free surface velocity (Benuzzi-Mounaix *et al.*, 2002). Another absolute EOS experiment is the symmetric impact method (Mitchell & Nellis, 1981; Knudson *et al.*, 2003; Nellis *et al.*, 2003).

Flyer plates are a common experimental tool to perform absolute EOS measurement in the gas-gun facilities (Mitchell & Nellis, 1981; Nellis *et al.*, 2003) and the *Z* machines Knudson *et al.* (2003). The success of those studies relies heavily on the condition of the flyer plate at impact. Gas-gun facilities have long produced ideal flyer plates. The *Z* machines have also achieved excellent results as well. Laser-driven flyer plate techniques have been demonstrated in high-power laser facilities for many years (Tanaka *et al.*, 2000; Ozaki *et al.*, 2001; Takamatsu *et al.*, 2003; Swift *et al.*, 2005). Laser-driven flyer techniques have distinct advantages. Such as laser-driven flyers can obtain higher flyer velocities and hence generate higher pressures. The sizes of the laser-driven flyer facilities are smaller, the experiments are less destructive, and therefore the corresponding experimental costs are lower. The laser ramp wave loading technique (Fratanduono *et al.*, 2012; Smith *et al.*, 2008) can accelerate a flyer plate to high velocity with low temperature. This is a potential technique that may be used to perform absolute EOS measurement in laser facility.

Address correspondence and reprint requests to: Hua Shu, Shanghai Institute of Laser Plasma, Shanghai 201800, China. E-mail: shuhua1979@163.com

In this paper, we performed an absolute EOS measurement on the principal Hugoniot of aluminum using a laser-driven flyer plate. An aluminum flyer plate of ~25 μm thick was accelerated to the velocity range from 4 to 12 km/s using the quasi-isentropic driving method. The aluminum flyer plate propagates across a vacuum gap and impacts with an aluminum step target. A line-imaging optical recording velocity interferometer for any reflector (ORVIS) is used to measure the velocities of the aluminum flyer plate and the shock wave simultaneously. Aluminum EOS data were measured with pressures range from 50 to 200 GPa.

2. EXPERIMENTAL SETUP

The experiments were performed using the "SG-II" Nd: Glass laser (converted at $\lambda = 0.527$ μm) of the National Laboratory on High Power Laser and Physics in ShangHai. The "SG-II" Laser facility provides one-dimensional (1D) compression by smoothed laser beams with short wavelength and high intensity. The temporal profile of the laser is nearly square with a rise and fall time of ~300 ps and a full-width at half-maximum (FWHM) of ~4 ns. Lens-array (LA) (Deng *et al.*, 1986; Fu *et al.*, 1995) was used to eliminate the large-scale spatial modulation and to obtain a flat-topped profile in the focal plane. Characteristics of the optical system (Lens + LA) were such that the focal spot had a flat region of $\sim 1.5 \times 1.0$ mm^2. The focal spot image of the laser is shown in Figure 1. The profile shows a flat top region of 1.5 mm with RMS non-uniformity <2%. Thanks to the LA, a good flyer with large planetary region can be obtained. The absorbed laser intensity in the focal spot is between ~1 and 3×10^{13} W/cm^2. The experimental setup is shown in Figure 2.

3. TARGET PRODUCTION

A double-cavity step target, with the structure sketched in Figure 3, was used in our experiment. The target is made up of a polyimide plate, a long vacuum gap, an aluminum flyer plate, a short vacuum gap, and an aluminum step. The polyimide plate thickness is in the range from 120 to 160 μm. The long vacuum gap distance is in the range from 200 to 300 μm. The aluminum flyer plate is about 25 μm. The short vacuum gap distance is in the range from 80 to 120 μm. The aluminum step is made of two thin foils. Foils of polycrystalline aluminum of 99.99% purity having nominal thickness of ~20 μm were used in the experiment. Samples were measured to be fully dense (2.71 g/cm^3) to within an accuracy of 1%. The foil thickness uniformity is less than 0.5% d (d is the thickness of the foil). A white-light interferometer was used to measure the step thickness. Foils with surface roughness <100 nm were selected to make the target.

4. DIAGNOSTIC INTRODUCTION

The principal diagnostic was a line-imaging ORVIS system (Celliers *et al.*, 2004; Shu *et al.*, 2012). The schematic optical setup of the system is shown in Figure 2. The first part of the imaging relay system (L1 and L2) produces a magnified real image at IP1. The magnification of this stage is 9.5×. L1 is composed of four achromatic lenses. This combination has 142 mm focal length and focal ratio $F/3$. L3 recollimates the beam for the path segment leading from the intermediate image (IP1) and through a periscope system onto the optical table, where it reaches L4. A set of two-beam splitters and a mirror are placed in the paths beyond lens L4.

The output images (IP2) are formed 1100 mm beyond lens L4 and the M–Z interferometers are placed precisely such that these images are simultaneously coincident with the output beam splitter in the interferometer. L5 recollimates the beam for the path segment leading from IP2, and through a Dove prism and reaches L6. At last, an output image is formed on the slit of the streak camera. The slit width of the streak camera is ~30 μm. The Dove prism is used to rotate the image to make the direction of the fringes align

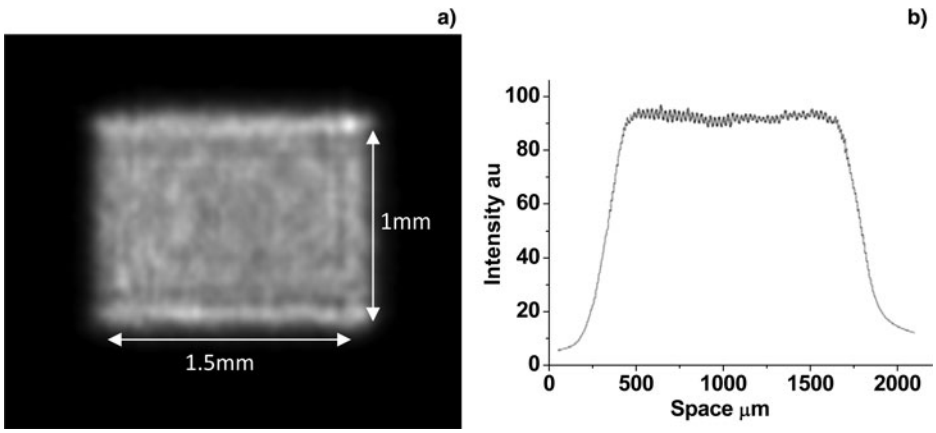

Fig. 1. The image of the laser focal spot: (a) two-dimensional image of the laser intensity on the focal plane; (b) one-dimensional laser intensity distribution profile on the focal plane.

https://doi.org/10.1017/S0263034616000896 Published online by Cambridge University Press

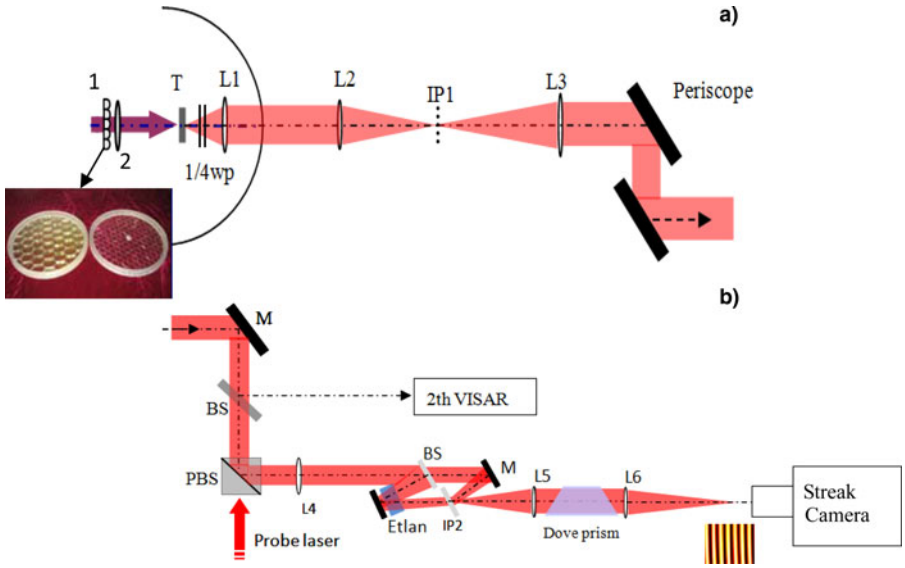

Fig. 2. Schematic representation of the experiments setup: 1. Lens-arrays; 2. Focus lens; T, target; L1–L6, lens; IP1, IP2, image plane; M, mirror; PBS, BS beam splitter.

with the silt of the visible streak camera. The total magnification of the image system is about 12×. Figure 4 shows the optical system alignment capability. A resolution pattern was placed at the target chamber center (TCC) and the minimum scale of the resolution pattern is 7 μm.

The streak camera sweeping non-linearity and temporal resolution are carefully calibrated using a Fabry–Pérot etalon (FP) and a laser with the wavelength of 0.53 μm and pulse width of ~1 ps. In the temporal resolution calibration experiment, the distance of the FP etalon was decreased continually until two adjacent signals cannot be distinguished, the double pass duration of the FP etalon [Fu *et al.* (2007)] is just the time resolution. The Rayleigh criterion is regarded as the judgment standard. Namely two adjacent signals cannot be distinguished when the superposition intensity between them reaches 73.5% of the peak intensity of the lower intensity one of them. The temporal resolution of the streak camera is about 220 ps in the 100 ns time window.

The ORVIS measures the aluminum flyer plate and the shock velocity simultaneously. In most shots, the etalon thickness is 45 mm corresponding to the velocity sensitivity of 1.25 km/s per fringe. In one shot, the etalon thickness is 18 mm corresponding to the velocity sensitivity of 3.0 km/s per fringe. The ORVIS data are analyzed with a FFT (fast Fourier transform) method that establishes fringe position to ~10% of a fringe. The probe laser for ORVIS is a Q-switched laser operating at 660 nm with a pulse length of 60 ns at FWHM. The reflected probe signal was recorded by a visible streak camera.

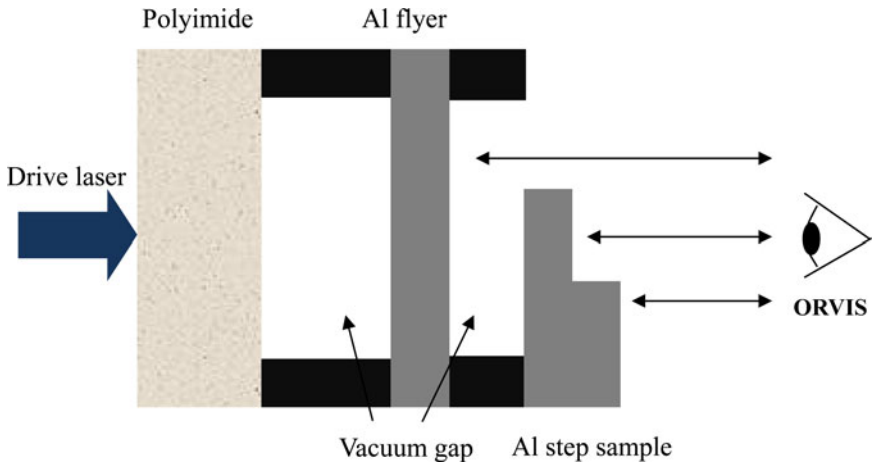

Fig. 3. Schematic representation of the target. The SG-II laser ablates a polyimide sample driving a strong shock. When the strong-shock emergence from the rear surface, causing the polyimide to unload as plasma across a vacuum gap. The aluminum flyer plate is ramp accelerated by the unloading plasma. The aluminum flyer plate propagates across a vacuum gap and impact with an aluminum step.

https://doi.org/10.1017/S0263034616000896 Published online by Cambridge University Press

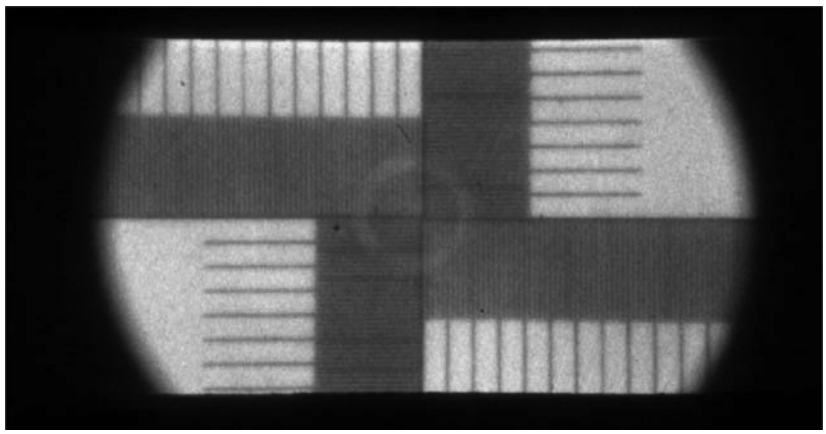

Fig. 4. Resolution pattern image, the minimum scale of the resolution pattern is 7 μm.

5. DRIVE PLANARITY

The experiment consists of four distinct phases. First, a strong shock is generated in the polyimide plate by the laser. After the shock exits the rear side of the polyimide, the plasma unloads toward the sample, expands along the first vacuum gap. Then the plasma piles up against an aluminum flyer and smoothly accelerates it. In the final phase, the aluminum flyer near-symmetrically impacts with the aluminum step target.

The planarity of the flyer is important for the measurement of the EOS. The planarity of the flyer is affected by the shock planarity in the polyimide, the planarity of the plasma piston and the flight time of the flyer. In order to obtain a plane shock wave, the beam smoothing technology of LA (Deng *et al.*, 1986; Fu *et al.*, 1995) was used. The LA was composed of an array of nearly 100 similar small lenses (see Fig. 2). This combination focus system makes the driving laser intensity uniformly distributed in space on the target. The LA is located in front of a principal lens (see Fig. 2). Characteristics of the optical system (Lens + LA) were such that the focal spot had a flat region of $\sim 1.5 \times 1.0$ mm. Figure 5 shows the shock break from a 35 μm Al foil. The root-mean-square deviation (RMS) of shock breakout time on varied space was used as an evaluation criterion of shock wave planarity. The variation of the shock breakout time RMS = 10 ps.

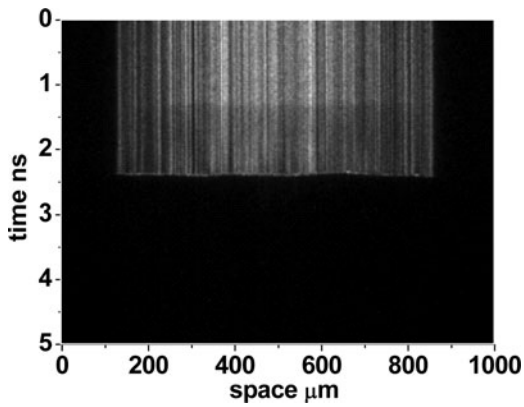

Fig. 5. Streak image of shock break out an Al flat target, the Al thickness is 30 μm.

The flyer is accelerated by the plasma piston, so the planarity of the plasma will affect the flyer planarity. It is difficult to directly observe the evolution of the planarity of the plasma piston with time. However, it is easy to observe the evolution of the planarity of the flyer with time. The flyer plate planarity is observed using the ORVIS. Figure 6 shows the ORVIS fringe image of a 25 μm-thick aluminum flyer. The central flat region of the flyer was larger than 600 μm diameter, with a variation in time RMS = 80 ps. The planarity of the flyer will become worse as the propagation time increases.

Figure 7 shows the ORVIS measurement result of a stepped aluminum target impacted by an aluminum flyer. The variation of the shock breakout time is RMS = 130 ps.

6. EXPERIMENTAL RESULTS

Figure 8a shows a typical ORVIS image of the experiment. The ORVIS views the aluminum flyer plate and step target simultaneously. The flyer velocity is diagnosed with an ORVIS and the shock velocity in the sample is determined from the breakout time of the shock across the step. The horizontal lines are the ORVIS fringes, and its vertical position is proportional to the velocity. Before $t \approx 28$ ns, the fringes are horizontal, that mean no velocity change. Then ($t \approx 28$ ns) the fringes begin to move, which represents the arrival of plasma piston. At $t \approx 57$ ns, the flyer plate is accelerated to a velocity of ~ 4.22 km/s and then impacts with the aluminum step target. At $t \approx 59$ ns, the shock emerges from the aluminum "base". At $t \approx 61$ ns, the shock emerges from the aluminum step. The shock and the flyer plate velocity can be clearly determined. Figure 9a shows another ORVIS image of the experiment. In this shot, the flyer plate is accelerated to a velocity of ~ 7 km/s. The derived flyer plate velocity histories show that the flyer is accelerated smoothly and shocklessly. Five shots were fired, and the results are listed in Table 1. Figure 10 shows all the flyers velocity profiles.

https://doi.org/10.1017/S0263034616000896 Published online by Cambridge University Press

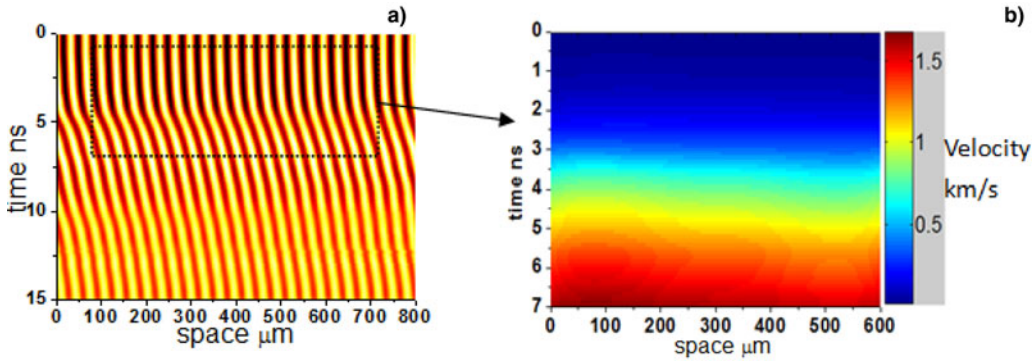

Fig. 6. (a). ORVIS image of a 25 μm-thick aluminum flyer; (b) velocity map, horizontal direction is the space, vertical direction is the time, color code is the velocity.

When the shock velocities and the particle velocities are obtained, the Hugoniot data of the sample can be determined. The measured Hugoniot data of aluminum are listed in Table 2.

The shock velocities measurement uncertainty comes from errors in determining the time intervals and the step thickness. In this experiment, the error in determining the time interval plays a major role. The error of time intervals derives mainly from the reading uncertainty. In our experiments, this uncertainty is about 250–300 ps. The shock wave travel time in the step is about 2–3 ns. Hence, the uncertainties in the shock velocities are about 10%. Uncertainties in the flyer plate velocities are decided by errors in ORVIS measurement. The ORVIS measurement uncertainty comes from errors in the probe laser wavelength, etalon thickness, and image processing, among which the last item plays a major role. The image-processing error is related to the rate of signal to noise of the image. In these experiments, the relative uncertainty for a fringe identification is about 10%. The velocity-per-fringe (VPF) constants are 1.25 and 3.0 km/s,

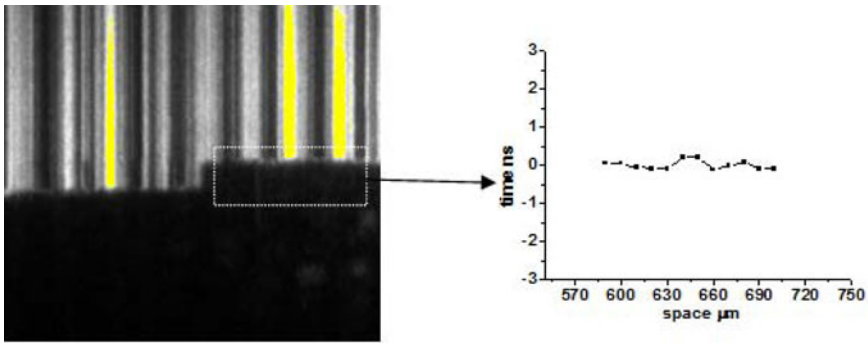

Fig. 7. Streaked ORVIS records of shock break out in a stepped aluminum targets.

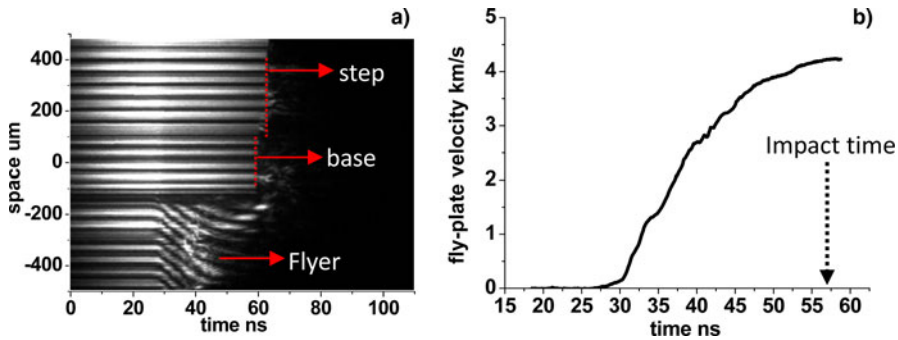

Fig. 8. (a) ORVIS fringe data for shot 25. Before $t \approx 28$ ns, the fringes are horizontal and constant because the fly-plate has not moved. After $t \approx 28$ ns, the fringes begin to move, which means that the fly-plate is accelerated. At $t \approx 57$ ns, the fly-plate is accelerated to a velocity of ~4.22 km/s, and then impacts with the aluminum step target. At $t \approx 59$ ns, the shock emergence from the aluminum "base". At $t \approx 61$ ns, the shock emergence from the aluminum step.

https://doi.org/10.1017/S0263034616000896 Published online by Cambridge University Press

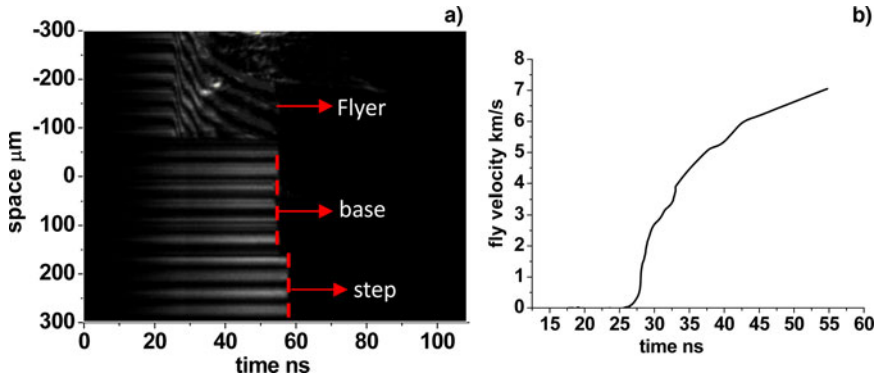

Fig. 9. (a) ORVIS fringe data for shot 26. Before $t \approx 20$ ns, the fringes are horizontal and constant because the flyer plate has not moved. After $t \approx 20$ ns, the fringes begin to move, which means that the flyer plate is accelerated. At $t \approx 54$ ns, the flyer plate is accelerated to a velocity of ~7 km/s, and then impacts with the aluminum step target. At $t \approx 56$ ns, the shock emergence from the aluminum "base". At $t \approx 58$ ns, the shock emergence from the aluminum step.

Table 1. *Aluminum principal Hugoniot results*

Shot no.	Step thickness (μm)	Transit time (ns)	Shock velocity (km/s)	Flyer velocity (km/s)
25	20.40 ± 0.06	2.43 ± 0.27	8.40 ± 0.93	4.22 ± 0.11
26	21.30 ± 0.07	2.14 ± 0.27	9.95 ± 1.40	6.99 ± 0.18
28	20.50 ± 0.062	2.25 ± 0.28	9.10 ± 1.13	5.50 ± 0.14
29	20.30 ± 0.06	1.62 ± 0.26	12.53 ± 2.0	11.58 ± 0.29
30	30.00 ± 0.072	3.37 ± 0.29	8.90 ± 0.77	5.08 ± 0.13

Measured shock velocity and flyer plate velocity.

suggesting a 4–5 fringes shift corresponding to the 12 km/s flyer velocity. The velocity uncertainties of the flyer plate are about 2–3%. The detailed experimental uncertainties analysis method is same as the literature (Fu *et al.*, 2007).

As a common interesting material, aluminum has been studied extensively by a lot of authors with various techniques (McQueen *et al.*, 1970; Marsh, 1980; Mitchell & Nellis, 1981; Knudson *et al.*, 2003). A summary of the shock velocity D and particle velocity u of aluminum with pressures range from 50 to 200 GPa from this work and other work is shown in Figure 11. Figure 12 shows the obtained shock pressure and shock density along with the Hugoniot data in the literature (McQueen *et al.*, 1970; Marsh, 1980; Mitchell & Nellis, 1981; Knudson *et al.*, 2003). The results of this work are in agreement with previously reported data within the experimental errors (Appendix).

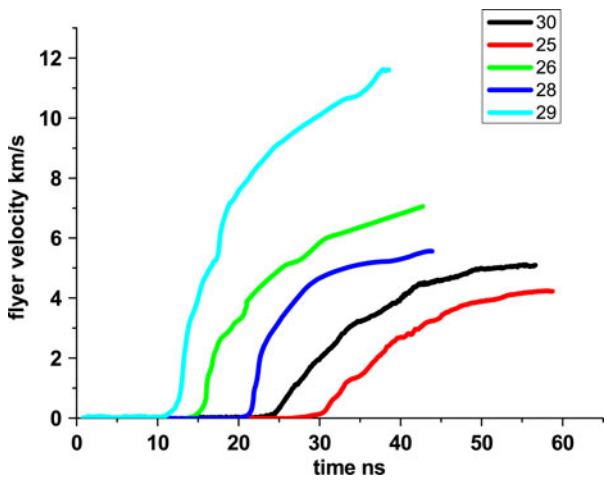

Fig. 10. The velocity profiles for all the flyers.

7. DISCUSSION

It is an attempt to perform absolute Hugoniot measurement using near-symmetric impact method using a laser-accelerated flyer plate. The uncertainty of the shock velocity is large. Uncertainties in the shock velocities come from errors in determining the time intervals and the step thickness. In this experiment, the error in determining the time interval plays a major role. In our experiment, only one streak camera was used. In order to observe the whole acceleration process of the flyer (~30 ns), a long-time window (~100 ns) is used in the experiment. The temporal resolution of the streak camera is about 220 ps at this sweep range. However, the shock across time in the step is about 2–3 ns. The uncertainty of the shock velocity can be reduced by using two streak cameras. One camera works in a long-time window (100 ns) to observe the whole acceleration process of the flyer. Another streak camera works in a short-time window (5 ns) to determine the shock across time in the step. The temporal resolution is about 20 ps at 5 ns sweep range. Hence, very rough estimation, the shock velocity uncertainty can scale down in the ratio of one to ten.

In order to obtain more accurate EOS data in the high-pressure range, we need to think about these issues, such as improving the flyer planarity and preventing the flyer preheat. The flyer planarity can be improved by improving the laser beam smoothing technique or using multi-laser beams. The main mechanism of preheating is the shock heating during the acceleration process and the thermal conduction heating by the plasma piston collide with the flyer. By

https://doi.org/10.1017/S0263034616000896 Published online by Cambridge University Press

Table 2. *Aluminum principal Hugoniot results*

Shot no	Flyer velocity (km/s)	Shock velocity (km/s)	Particle velocity (km/s)	Shock pressure (GPa)	Shock density (g/cm^3)
25	4.22 ± 0.11	8.40 ± 0.93	2.11 ± 0.11	48.0 ± 6.0	3.6 ± 0.2
26	6.99 ± 0.18	9.95 ± 1.40	3.45 ± 0.18	94.2 ± 14.1	4.2 ± 0.3
28	5.50 ± 0.14	9.10 ± 1.13	2.75 ± 0.14	67.8 ± 9.1	3.9 ± 0.2
29	11.58 ± 0.29	12.53 ± 2.0	5.79 ± 0.29	196.6 ± 33.0	5.0 ± 0.7
30	5.08 ± 0.13	8.90 ± 0.77	2.54 ± 0.13	61.3 ± 6.3	3.8 ± 0.2

Inferred shock pressure and shock density.

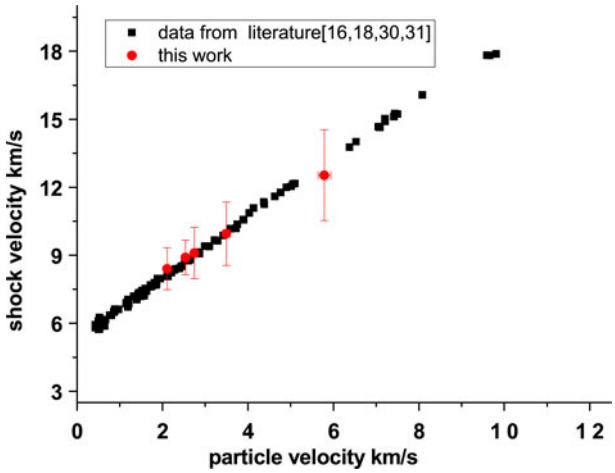

Fig. 11. Comparison of the shock velocity and particle velocity of aluminum determined from this work and literature (McQueen *et al.*, 1970; Marsh, 1980; Mitchell & Nellis, 1981; Knudson *et al.*, 2003).

optimizing design, the flyer can be accelerated smoothly. Thermal conduction heating may be reduced by adding a plastic preheating shield in front of the flyer. By optimizing, high-quality and high-speed flyer plate may be obtained to perform high-pressure absolute EOS studies using high-power laser facility.

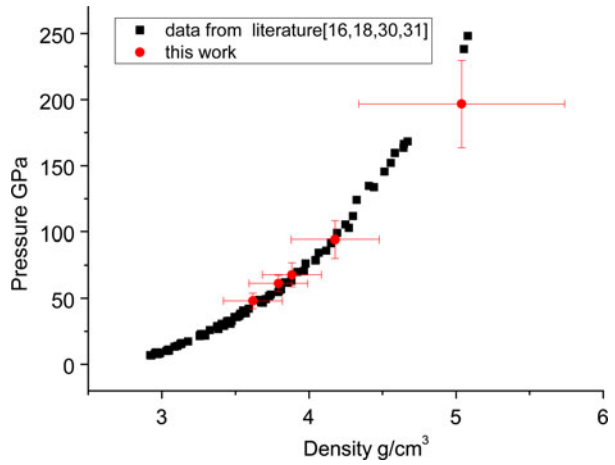

Fig. 12. The obtained shock pressure and shock density along with the Hugoniot data in the literature (McQueen *et al.*, 1970; Marsh, 1980; Mitchell & Nellis, 1981; Knudson *et al.*, 2003).

8. CONCLUSION

In conclusion, we have performed an absolute EOS measurement on the principal Hugoniot of aluminum using a near-symmetric impact method. An aluminum flyer plate of ~25 μm was accelerated to the velocity range from 4 to 12 km/s using the quasi-isentropic driving method. Then the aluminum flyer plate propagates across a vacuum gap and impacts with an aluminum step target. A line-imaging ORVIS is used to measure the aluminum flyer plate velocity and the shock velocity simultaneously. Aluminum EOS data were measured with pressures from 50 to 200 GPa. The results of this work are in agreement with the previously reported data in a comparable pressure regime with various techniques. This absolute EOS measurement method may be used for studying a variety of materials.

ACKNOWLEDGMENT

The authors gratefully acknowledge the valuable support for the experiments by the "SG-II" technical crews.

REFERENCES

Batani, D. (2016). Matter in extreme conditions produced by lasers. *Europhys. Lett.* **114**, 65001.

Batani, D., Strati, F., Stabile, H., Tomasini, M., Lucchini, G., Ravasio, A., Koenig, M., Benuzzi-Mounaix, A., Nishimura, H., Ochi, Y., Ullschmied, J., Skala, J., Kralikova, B., Pfeifer, M., Kadlec, C., Mocek, T., Prag, A., Hall, T., Milani, P., Barborini, E. & Piseri, P. (2004). Hugoniot data for carbon at megabar pressures. *Phys. Rev. Lett.* **92**, 065503.

Benuzzi, A., Löwer, T., Koenig, M., Faral, B., Barani, D., Beretta, D., Danson, C. & Pepler, D. (1996). Indirect and direct laser driven shock waves and applications to copper equation of state measurements in the 10–40 Mbar pressure range. *Phys. Rev. E* **54**, 2162.

Benuzzi-Mounaix, A., Koenig, M., Huser, G., Faral, B., Batani, D., Henry, E., Tomasini, M., Marchet, B., Hall, T.A. & Boustie, M. (2002). Absolute equation of state measurements of iron using laser driven shocks. *Phys. Plasmas* **9**, 2466.

Cauble, R., Perry, T.S., Bach, D.R., Budil, K.S., Hammel, B.A., Collins, G.W., Gold, D.M., Dunn, J., Celliers, P., Da Silva, L.B., Foord, M.E., Wallace, R.J., Stewart, R.E. & Woolsey, N.C. (1998). Absolute equation-of-state data in the 10–40 Mbar (1–4 TPa) regime. *Phys. Rev. Lett.* **80**, 1248.

https://doi.org/10.1017/S0263034616000896 Published online by Cambridge University Press

Celliers, P.M., Bradley, D.K., Collins, G.W., Hicks, D.G., Boehly, T.R. & Armstrong, W.J. (2004). Line-imaging velocimeter for shock diagnostics at the OMEGA laser facility. *Rev. Sci. Instrum*. **75**, 4916.

Celliers, P.M., Collins, G.W., DaSilva, L.B., gold, D.M. & Cauble, R. (1998). Accurate measurement of laser-driven shock trajectories with velocity interferometry. *Appl. Phys. Lett*. **73**, 1320.

Deng, X.M., Liang, X.C. & Chen, Z. (1986). Uniform illumination of laser targets using a lens array. *Appl. Opt*. **25**, 377.

Fratanduono, D.E., Smith, R.F., Boehly, T.R., Eggert, J.H., Braun, D.G. & Collins, G.W. (2012). Plasma-accelerated flyer-plates for equation of state studies. *Rev. Sci. Instrum*. **83**, 073504.

Fu, S.Z., Gu, Y., Wu, J. & Wang, S.J. (1995). Laser-driven shock stability in Al and shock compressibilities of Fe up to 0.8 TPa and SiO_2 up to 0.4 Tpa. *Phys. Plasmas* **9**, 3201.

Fu, S.Z., Huang, X.G., Ma, M.X. & Shu, H. (2007). Analysis of measurement error in the experiment of laser equation of state with impedance-match way and the Hugoniot data of Cu up to similar to 2.24 TPa with high precision. *J. Appl. Phys*. **101**, 043517.

Godwal, B.K., Rao, R.S., Verma, A.K., Shukla, M., Pant, H.C. & Sikka, S.K. (2003). Equation of state of condensed matter in laser-induced high-pressure regime. *Laser Part. Beams* **21**, 523.

Gu, Y., Fu, S., Wu, J., Yu, S., Ni, Y. & Wang, S. (1996). Equation of state studies at SILP by laser-driven shock waves. *Laser Part. Beams* **14**, 157.

Hann, S.W., Pollaine, S.M., Lindl, J.D., Suter, L.J., Berger, R.L., Powers, L.V., Alley, W.E., Amend, P.A., Futterman, J.A., Levedahl, W.K., Rosen, M.D., Rowley, D.P., Sacks, R.A., Shestakov, A.I., Strobel, G.L., Tabak, M., Weber, S.V., Zimmerman, G.B., Krauser, W.J., Wilson, D.C., Coggeshall, S.V., Harris, D.B., Hoffman, N.M. & Wilde, B.H. (1995). Design and modeling of ignition targets for the national ignition facility. *Phys. Plasmas* **2**, 2480.

Knudson, M.D., Lemke, R.W., Hayes, D.B., Hall, C.A., Deeney, C. & Asay, J.R. (2003). Near-absolute Hugoniot measurements in aluminum to 500 GPa using a magnetically accelerated flyer plate technique. *J. Appl. Phys*. **94**, 4420–4431.

Koenig, M., Benuzzi, A., Faral, B., Krishnan, J., Boudenne, J.M., Jalinaud, T., Remond, C., Decoster, A., Batani, D., Beretta, D. & Hall, T.A. (1998). Brominated plastic equation of state measurements using laser driven shocks. *Appl. Phys. Lett*. **72**, 1033.

Lindl, J.D. (1995). Development of the indirect-drive approach to inertial confinement fusion and the target physics basis for ignition and gain. *Phys. Plasmas* **2**, 3933.

Marsh, S.P. (Ed.). (1980). *LASL Shock Hugoniot Data*. Berkeley: University of California Press.

McQueen, R.G., Marsh, S.P., Taylor, J.W., Fritz, J.N. & Carter, W.J. (1970). The equation of state of solids from shock wave studies. In *High Velocity Impact Phenomena*, (Kinslow, R., Ed.), pp. 293–417. New-York: Academic Press; appendices on pp. 515–568.

Mitchell, C. & Nellis, W.J. (1981). Shock compression of aluminum, copper and tantalum. *J. Appl. Phys*. **52**, 3363.

Mithcell, A.C., Nellis, W.J., Moriarty, J.A., Heinle, R.A., Holmes, N.C., Tipton, R.E. & Repp, G.W. (1991). Equation of state of Al, Cu, Mo, and Pb at shock pressures up to 2.4 TPa. *J. Appl. Phys*. **69**, 2981.

Nellis, W.J., Mitchell, A.C. & Young, D.A. (2003). Equation-of-state measurements for aluminum, copper, and tantalum in the pressure range 80–440 GPa (0.8–4.4 Mbar). *J. Appl. Phys*. **93**, 304.

Ozaki, N., Sasatani, Y., Kishida, K., Nakano, M., Miyanaga, M., Nagai, K., Nishihara, K., Norimatsu, T., Tanaka, K.A., Fujimoto, Y., Wakabayashi, K., Hattori, S., Tange, T., Kondo, K., Yoshida, M., Kozu, N., Ishiguchi, M. & Takenaka, H. (2001). Planar shock wave generated by uniform irradiation from two overlapped partially coherent laser beams. *J. Appl. Phys*. **89**, 2571.

Ragan III., C.E. (1982). Shock compression measurements at 1 TPa to 7 TPa. *Phys. Rev. A* **25**, 3360.

Shu, H., Fu, S.Z., Huang, X.G., Wu, J., Zhou, H.Z. & Ye, J.J. (2012). A modified illumination system for a line-imaging optically recording velocity interferometer and its application in equation of state measurement. *Meas. Sci. Technol*. **23**, 015203.

Silva, L.D., Celliers, P., Collins, G.W., Budil, K.S., Holmes, N.C., Barbee, T.W., Hammel, B.A., Kilkenny, J.D., Wallace, R.J., Ross, M., Cauble, R., Ng, A. & Chiu, G. (1997). Absolute equation of state measurements on shocked liquid deuterium up to 200 GPa (2 Mbar). *Phys. Rev. Lett*. **78**, 483.

Smith, R.F., Eggert, J.H., Saculla, M.D., Jankowski, A.F., Bastea, M., Hicks, D.G. & Collins, G.W. (2008). Ultrafast dynamic compression technique to study the kinetics of phase transformations in bismuth. *Phys. Rev. Lett*. **101**, 065701.

Swift, D.C., Niemczura, J.G., Paisley, D.L., Johnson, R.P., Luo, S.-N. & Tierney IV., T.E. (2005). Laser-launched flyer plates for shock physics experiments. *Rev. Sci. Instrum*. **76**, 093907.

Takamatsu, K., Ozaki, N., Tanaka, K.A., Ono, T., Nagai, K., Nakai, M., Watari, T., Sunahara, A., Nakano, M., Kataoka, T., Takenaka, H., Yoshida, M., Kondo, K. & Yamanaka, T. (2003). Equation-of-state measurements of polyimide at pressures up to 5.8 TPa using low-density foam with laser-driven shock waves. *Phys. Rev. E* **67**, 056406.

Tanaka, K.A., Hara, M., Ozaki, N., Sasatani, Y., Anisimov, S.I., Kondo, K.-I., Nakano, M., Nishihara, K., Takenaka, H., Yoshida, M. & Mima, K. (2000). Multi-layered flyer accelerated by laser induced shock waves. *Phys. Plasmas* **7**, 676.

Vladimirov, A. (1984). Shock compressibility of aluminum at p greater-than-or-equal-to 1 Gbar. *JETP Lett*. **39**, 82.

APPENDIX: UNCERTAINTY ANALYSIS

The shock velocity D is obtained by

$$D = d/t, \tag{1}$$

where d is the sample step thickness, and t is the transit time of the shock wave in the step. Obviously, the uncertainty δD depends on the uncertainties d and t. Using the error transfer rule and Eq. (1), δD is given as

$$\delta D = D\sqrt{\left(\frac{\delta d}{d}\right)^2 + \left(\frac{\delta t}{t}\right)^2}. \tag{2}$$

In this experiment, the error in determining the time interval plays a major role. The error of time intervals derives mainly from the reading uncertainty. In our experiments, this uncertainty is about 250–300 ps. The shock wave travel time in the step is about 2–3 ns. Hence, the uncertainties in the shock velocities are about 10%. If the streak camera works in a fast sweep rate (5 ns time window), then the transit time determining error can be decreased.

https://doi.org/10.1017/S0263034616000896 Published online by Cambridge University Press

The shock pressure is inferred by

$$P = \rho_0 D u, \tag{3}$$

where ρ_0 is the sample initial density, D is the shock velocity, u is the particle velocity, and P is the shock pressure. The shock velocity and particle velocity are measured independently. The uncertainty δP depends on the uncertainties D and u. Using the error transfer rule and Eq. (3), δP is given as

$$\delta D = D\sqrt{\left(\frac{\delta d}{d}\right)^2 + \left(\frac{\delta t}{t}\right)^2}. \tag{4}$$

The shock density is inferred by

$$\delta P = \rho \frac{\sqrt{(D \times \delta u)^2 + (u \times \delta D)^2}}{D \times (D - u)}, \tag{5}$$

where ρ_0 is the sample initial density, D is the shock velocity, u is the particle velocity, and ρ is the shock density. Using the error transfer rule and Eq. (5), $\delta\rho$ is given as

$$\delta \rho = \rho \frac{\sqrt{(D \times \delta u)^2 + (u \times \delta D)^2}}{D \times (D - u)}. \tag{6}$$

https://doi.org/10.1017/S0263034616000896 Published online by Cambridge University Press